Geomechanics for Energy and the Environment 21 (2020) 100159

Contents lists available at ScienceDirect

Geomechanics for Energy and the Environment

journal homepage: www.elsevier.com/locate/gete

A study on bond breakage behavior of weak Cretaceous Kazakhstani reservoir sandstone analogue

Ashirgul Kozhagulova [a,*], Nguyen Hop Minh [b], Yong Zhao [a], Sai Cheong Fok [a]

[a] School of Engineering, Nazarbayev University, 53 Kabanbay batyr avenue, Astana, Kazakhstan
[b] Fulbright University Vietnam, 105 Ton Dat Tien, Ho Chi Minh City, Viet Nam

ARTICLE INFO

Article history:
Received 11 April 2019
Received in revised form 10 July 2019
Accepted 6 November 2019
Available online 12 November 2019

Keywords:
Weak sandstone
Cement bonding
Bonding degradation
Laboratory tests
Discrete element method

ABSTRACT

The study examines the effect of cement bond breakage in the mechanical behavior of porous weak sandstones in Kazakhstan's oil fields using one-dimensional compression, triaxial shearing apparatuses, and Discrete Element Method (DEM) numerical simulation. Analogue sandstone materials were prepared by cementing a sand material with similar mineralogy to the real reservoir with the sodium silicate solution. The results of the cemented sandstones were compared to the results of the uncemented sand, disaggregated sandstone and silty sand of similar particle size distribution to understand the effect of the cemented structure. The failure behavior of the material was investigated in the experimental and numerical studies at different confining pressures and it was found that the behavior is mainly controlled by the cement bonds as there is no major change in the particles during the tests. It was found that the plastic yielding condition is mainly associated with the breakage of the cement bonds and this gives rise to volume compression and strain hardening of the material. The DEM results provide further confirmation that the degradation of the specimen stiffness is directly related to the bond breakage initiation and higher confining pressures affect the breakage rate and weaken the effect of the cemented structure, which is compensated by a stronger role for the frictional resistance between sand particles.

1. Introduction

The behavior of weak sandstones is of high interest to the oil and gas industries in Kazakhstan as several local oil fields were found in shallow poorly consolidated formations. A better understanding of weak sandstone characteristics would not only lower the cost of oil recovery, but also minimize the ecological impact as severe sand production problems were encountered during the production process in these fields. The behavior of weak sandstones have been studied in the literature and the materials can be evaluated using soil mechanics theories such as the critical state soil mechanics.[1,2] The plastic deformation and strain hardening behaviors of weak sandstones are governed by the cemented structure, which can be transformed to a friction dominant state as the structure degrades.[3] Furthermore, the microscopic characteristics of the grain shape, packing, sorting, texture[4] as well as the grain size[4–6] were found to be factors affecting the strength and deformability characteristics of these weak rocks.

Although there are many studies on the characteristics of weak sandstones, there are limited investigations on the evolution of the cemented structure of these weak rocks. The structural changes of rocks can be caused by the combined response of the fabric and bonding during different stages of mechanical loading.[7] It is also recognized that the current classification of weak rocks is solely based on the value of the uniaxial compressive strength (UCS) with no distinction between different types of individual grains and interparticle cement. Therefore, a wide range of sandstones from carbonate sandstones comprised of weak particles[8] to sandstones of strong silica particles bonded by weak cement[3,9] can all be classified as weak rocks but yet they behave differently from each other.

Previous studies on weak sandstones included investigations into strong silica grains bonded with weak cement[3,9] as well as weak calcareous grains bonded with strong cement.[3,9,10] In particular, the role of bond breakage between weak calcareous grains had been examined.[10] This work extends upon their findings by examining the role of bonding during the structural changes for the weakly cemented porous sandstones of Kazakhstan. The weak reservoir sandstones in Kazakhstan are associated with Cretaceous deposits. While the materials usually possess high porosity and permeability and are classified as poorly consolidated sandstones in the industries, they consist of strong silica

* Corresponding author.
E-mail addresses: ashirgul.kozhagulova@nu.edu.kz (A. Kozhagulova), hopminh.nguyen@fulbright.edu.vn (N.H. Minh), yong.zhao@nu.edu.kz (Y. Zhao), sai.fok@nu.edu.kz (S.C. Fok).

https://doi.org/10.1016/j.gete.2019.100159
2352-3808/

particles and very weak cement bonding. As the material behavior is strongly influenced by the bonds and its breakage behavior, it is examined in this study by means of both experimental and numerical methods.

Due to the poor quality of the retrieved core samples from the oil-bearing formations, analogue specimens were prepared for mechanical testing such that the synthetic material possesses similar properties of the real reservoir rock in terms of strength, particle size distribution as well as porosity and permeability. Furthermore, bond breakage behavior of the artificial sandstone is studied using the Discrete Element Method[11] (DEM), which serves as a numerical analysis to investigate the behavior of granular assemblies through modeling the interaction at contacts between spherical particles, which are bonded in this case. The breakage behavior of bonds is simulated explicitly in this case, which is different from the continuum-based approach where bond degradation is considered as an internal variable.[12] The Discrete Element Method had been successfully used to study the behavior of sandstones in the literature where the bond behaviors were simulated by different contact models and techniques.

Wang and Leung[8] simulated triaxial tests of cemented sand with Portland cement using the commercial software PFC2D, where the cement particles were simulated as special tiny disks that form parallel bonds with the sand particles. Using the same two dimensional DEM software, Utili and Nova[13] developed a new contact bond model based on the Mohr–Coulomb failure criteria to simulate a strong bond behavior where the bond strength is dependent on the interparticle cohesion and the interparticle friction angle. In Shen et al.,[14] a complex contact bond model was developed for three-dimensional DEM simulation of spherical particles, where the bond behavior is considered in great detail including the bond geometry, pre-breakage and post-breakage behaviors of the bonds.

For the weak artificial sandstone in this study, the bonds are considered fragile, the effect of which on the macroscopic material behavior diminishes quickly after the peak strength. The behavior of the weak sandstone can be captured in an efficient computational simulation using a simple contact bond model based on the JKR model[15] as proposed by Rakhimzhanova et al.[16,17] The same method is utilized for the three dimensional DEM simulation of bonded spherical sand particles in this study. The results show a good agreement with the experimental behavior and provide new information on the bond breakage behavior at the contact level. The study of the effect of bonding to apprehend the mechanical behavior of the weak porous sandstones is critical for understanding the sanding problem and finding a better solution for the minimization of the sand production in the local oil fields.

2. Experimental program

Core sampling of weak natural sandstones has been known to be challenging.[4] The experimental studies were performed on specimens of artificial sandstone replicating the natural materials in the field as the retrieved field core samples were of the very poor quality and unsuitability for mechanical testing. Specimen preparation process involved bonding sand similar to field sand mineralogy with silicate solution while maintaining certain features of the real sandstone in terms of the grain size distribution, porosity value of 33%∼35%, permeability value of 500∼700 mD and the strength value similar to the reservoir rock of interest with UCS of 600∼700 kPa. The sample preparation procedure was adopted from Refs. 18–21. The cementation process, however, was accomplished with no confinement applied on the specimen so that the material remains weak and porous, replicating the real reservoir rock.

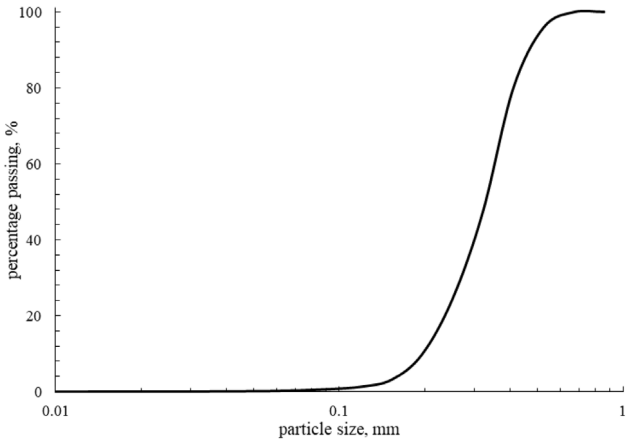

Fig. 1. Particle size distribution of the open-quarry quartz sand used in the artificial sandstone preparation.

2.1. Sample preparation method

Fig. 1 shows the cumulative particle size distribution of an open-quarry quartz sand used in this study. Based on the granulometric analysis the material is classified as poorly graded sand according to the unified classification system.[22] The sand has a mean grain size D50 of 0.32 mm with a specific gravity of 2.65. The microscope image of the sand in Fig. 2a shows sub-rounded particles and EDS spectrum confirmed pure quartz composition.

The sample preparation method was adopted from literature[18–21] but modified to prepare samples of lower strength and weaker cement bonds. Furthermore, the method was modified such that it can be applicable to prepare samples of consistent material behavior for element tests and for a sand production experiment of much larger cylindrical samples under fluid flow and boundary stress conditions as similar to the field. Since the material is weak to the extent that the real cores were damaged beyond the possibility of any reliable mechanical testing on these samples, the behavior of intact material is investigated here and the effect of core damage due to unloading–reloading during core retrieving is not considered as opposed to the studies by Holt et al.[20,21] Compared to the real cores, the condition of the synthetic material in this study should be closer to the undisturbed condition of the in-situ materials in an ideal case.

Sand to cement ratio by mass of 100:10 was used for specimen preparation, sand and silicate solution were weighted according to the target proportions and mixed thoroughly. The sample B300 (see Table 1) of the 100:10 sand cement ratio, for example, was prepared by mixing 300 g of sand with 30 g of cement. The mixture was kept in an air-tight container to avoid reaction with carbon dioxide in the air and then transferred to a split mold layer by layer. Each layer was lightly compacted and its surface was scratched before starting the next layer to ensure that there is no distinct boundary between the layers. This technique had been used in previous works[23–25] to provide uniformity of the material and avoid lamination and bedding effects. After the top layer was placed, a small static compaction was applied to the whole specimen. The hardening process of the cementation was initiated by injecting carbon dioxide gas from the end planes to the specimen, which was still being kept within the split mold, and the chemical reaction should occur as follows:.

$$Na_2Si_3O_7 + 2CO_2 + 2H_2O = 2NaHCO_3 + 3SiO_2xH_2O \quad (1)$$

Injecting the carbon dioxide may not be sufficient for the uniform hardening of the cement as this could result in a hardened

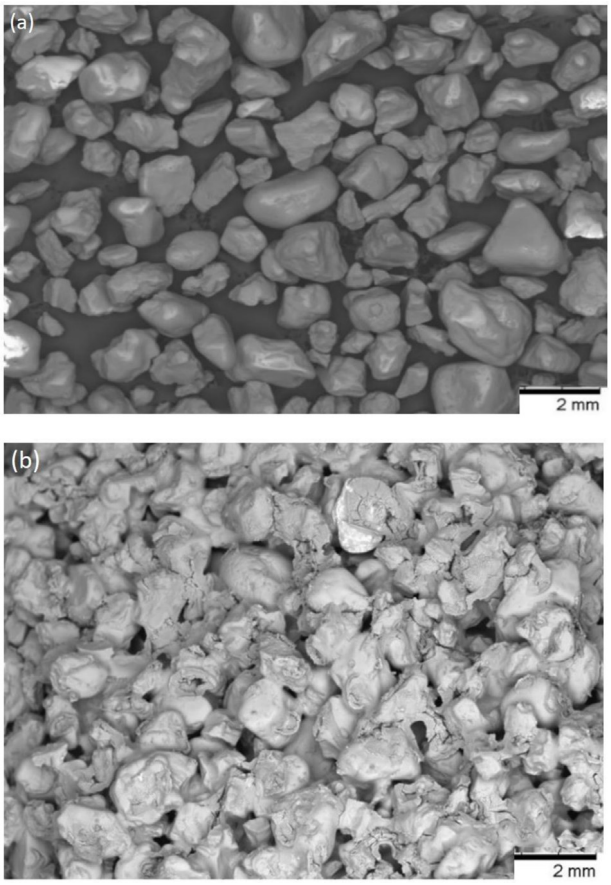

Fig. 2. Open quarry sand: (a) before and (b) after cementation.

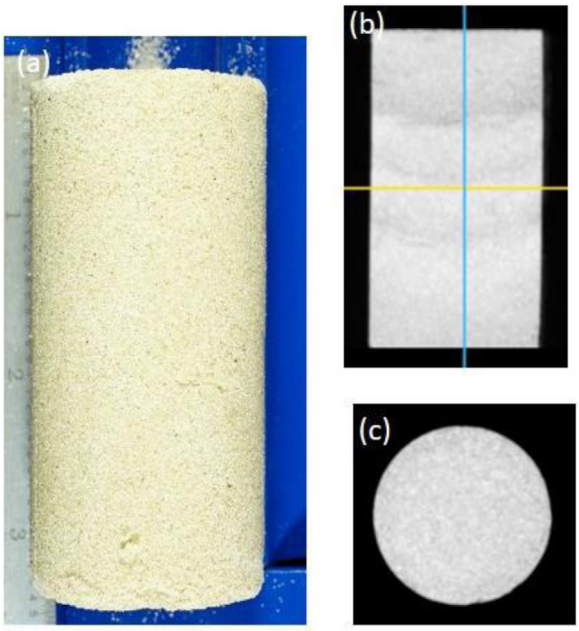

Fig. 3. X-ray CT Images of artificial sandstone: (a) general view; (b) axial section of XRCT; (c) cross-section of XRCT.

outer surface with a softer inner core. The CO_2 gas has to invade through the pores and circulate through the specimen. This was accomplished by removing the sample from the mold and placing it in a positive pressure metal chamber, which was maintained at an ambient pressure of 2 bars for 5 min. In the scanning electron microscopy image of the cemented sand in Fig. 2b, the cement bonding is formed as a homogeneous cement blanket covering both the surface of the sand grains and the spaces between them. There is no visible crack in the cement in the captured image, which means that the bonding remained intact as we moved the specimen around and bond breakage would depend on the subsequent loading conditions applied on the specimen during the tests.

Further information on the sample preparation and the effect of cement content on the uniaxial compressive strength can be found in previous work of the authors.[26]

The homogeneity of the artificial sandstone specimens was checked with the X-ray Computer Tomography (X-ray CT) Multislice CT Scan 128 SLICE from PHILIPS as shown in Fig. 3. The measurements were taken every 0.67 mm through the length of the sample with the scanning speed of 0.56 cm/s. The scanning of the specimen reveals some features otherwise not visible to the naked eyes. The axial sections of X-ray CT images show an acceptable horizontal bedding effect and little inhomogeneity in terms of porosity in the longitudinal direction. In the lateral direction from the central axis of the specimen towards the periphery the cement distribution is fairly homogeneous, therefore described sample preparation technique was accepted for this study.

For the oedometer tests, the specimens were prepared to have different initial specific volumes. The samples were prepared directly inside the cutting ring, in order to eliminate the gap between the specimen and the ring and to minimize the disturbance and interference while transferring the material. To compare with the results of the cemented sandstone, four types of uncemented specimens were also tested to examine the effects of the initial cemented structure and the effects of slightly different particle size distribution and particle characteristics between the two cemented and uncemented materials as follows:

- Loose uncemented sand sample prepared without compaction;
- Dense uncemented sand sample prepared with compaction;
- Silty sandstone sample prepared by mixing the original open quarry sand with mortar milled sand in ratio of 100:10;
- Disaggregated sandstone sample prepared by gently breaking the cement bonds of the cemented sandstone.

2.2. Test conditions

In the one-dimensional compression test, the samples were vertically compressed to high stress levels using a 24 mm diameter oedometer ring. The cemented samples were tested using a floating ring configuration, which minimizes the effect of boundary friction,[27] whereas the uncemented samples including both the loose and dense uncemented sand samples, disaggregated sand samples, and silty sand samples were subjected to the compression in a cell with a fixed ring of the same diameter.

Triaxial compression tests were conducted on uncemented sand (specimen type A) and cemented sandstone (specimen type B) under the following conditions as given in the summary in Table 1:

– monotonic loading: tests A300, B300, B400, B500, B700 are drained tests, which were sheared at a constant loading rate of 0.0125% strain/min with the associated numeric values indicate confining pressure in the low to medium ranges;

– cyclic loading: test B850 is a drained shear test at constant mean stress which includes three loading unloading probes to investigate the effect of bonding breakage before the peak strength and then the test was continued by normal hearing until large deformation;

Table 1
Summary of triaxial tests.

Test	Cementation	Void ratio	Confining pressure (p_c, kPa)	Peak strength (q_{peak}, kPa)	Utilization of internal LVDT
Monotonic loading – low to medium confining pressure					
A300	Uncemented	0.579	300	973	No
B300	Cemented	0.525	300	1597	No
B400	Cemented	0.485	400	1825	No
B500	Cemented	0.514	500	2244	No
B700	Cemented	0.474	700	2455	Yes
Cyclic loading – medium confining pressure					
B850	Cemented	0.481	850	2358	Yes
Monotonic loading – high confining pressure					
B4200	Cemented	0.774	4200	Not reached	Yes

– monotonic loading: test B4200 is a drained test at higher confining pressure with a constant loading rate.

The triaxial compression tests of the low and medium confining pressure were carried out using the standard triaxial apparatus in our laboratory where the axial load was measured by a load cell located inside the triaxial chamber with a capacity of 10 kN and a minimal resolution of 0.01 kN.

The medium stress tests (B700, B850) were conducted at the Department of Civil, Environmental and Geomatic Engineering of the University College London in the United Kingdom, where the equipment is computer-controlled and the axial strain was measured by both external and internal LVDTs (Table 1), which allowed the measurement of the initial strains with a resolution smaller than 1 μm for more accurate calculation of the initial stiffness. Sample B4200 was tested with the help of Schlumberger Reservoir Laboratories in Calgary, Canada. Both axial strain and radial strain were measured in triaxial test. The specimen was saturated with water and tested at room temperature with an effective confining pressure of 4200 kPa under drained condition.

The triaxial tests were conducted following procedures described in the British Standard.[28] Saturation stage was achieved when the pore pressure coefficient B value reached 0.95 and above[29] and we proceeded to consolidation stage with the effective confining pressure as given in Table 1 and finally the samples were sheared under drained condition until failure. The void ratio values were determined based on the initial dimensions and weight of the sample and checked through back-calculation using the final moisture ratio.[30] For the specimens that showed post-peak bulging and planar shear failure, the area correction[31] was used for calculating the stress values.

In addition to the mechanical testing of the material, we measured individual particle characteristics using the Sympatec particle analyzer QICPIC, which captures particle images and conducts statistical analysis of the size distribution and particle geometrical properties. The measured particles were fed into the dry dispersion unit RODOS via the dosing unit at a constant mass flow, compressed air was used to disperse the particles and the particles flow through the scanning beams emitted by a pulsed laser. The device captures particle sizes ranging from 0.1 μm to 4000 μm.

3. Compression

The compressional behaviors of granular soils have been extensively studied in the literature and the results indicated that volume compression of granular materials is significant due to particle breakage.[27,32,33] Breakage of sand particles usually start in the stress ranges between 10 and 100 MPa.[34] depending on the stiffness of individual grains for cemented sandstones, Cuccovillo & Coop[9] studied two cemented materials with one material consisted of strong particles with weak cements and another one of weak particles and strong cements. The results of isotropic compression showed that for strong cements, the normal compression line (NCL) that describes the volume compression of the cemented sand in term of the specific volume (v) as a function of the applied mean pressure (p') is located to the right of the NCL of the uncemented sand (i.e., higher stresses) in the (v:lnp') space; the weak cements on the other hand would move the cemented NCL to the left of the uncemented one (i.e., lower stresses).

To study the behavior of our artificial cemented sandstone and of the silica cement bonds, the oedometer tests were conducted on cemented sandstone and uncemented specimens of sand, silty-sand and disaggregated sandstone. The results are plotted in Fig. 4 in terms of v versus lnp' where the mean stress values are estimated from the applied vertical stress and the calculated horizontal stress using the at-rest earth pressure coefficient values $K_0 = 0.40$ and $K_0 = 0.44$ for cemented and uncemented materials, respectively. The value of K_0 was precalculated using the Jaky's equation[35] such that $K_0 = 1 - \sin\phi'$ where ϕ' is the peak frictional angle measured for both materials in our laboratory experiments.

The Jaky's equation, $K_0 = \sigma'_h/\sigma'_v = 1 - \sin\phi'$, is generally accepted to provide a good estimation of the at-rest horizontal stress ratio under one dimensional compression condition, and within the stress levels that do not allow plastic particle deformation to take place.[36] While the at-rest condition indicates a stress state below the failure condition, the K_0 value is related to the peak frictional angle (ϕ') at failure, which can be calculated from the experimental results as follows:

$$\sigma_1^{/} - \sigma_3^{/} = 2^{*}c^{*}cos\phi' + (\sigma_1^{/} + \sigma_3^{/})^{*}sin\phi', \quad (2)$$

where c - cohesion intercept, kPa

ϕ'- peak frictional angle, degrees

$\sigma_1{}^{/}$, $\sigma_3{}^{/}$ - major and minor effective principle stresses at the peak strength, kPa

The frictional angle was calculated to be $\phi' = 38.3^0$ with cohesion intercept equal to 120 kPa.

The compression curves of the cemented sandstone and of the disaggregated sandstone are shown in Fig. 4a, the main difference between them are the cemented structure, as otherwise their particle size distributions would be identical as of a mixture of sand particles and cement particles. Regardless of the initial specific volume, the compressional curves of the cemented sandstone converge into a unique Normal Compression Line (NCL), which can be approximated by the following equation:

$$v = N_0 - \lambda^{*} ln\ p^{/} \quad (3)$$

where $N_0 = 2.987$ is the intercept of the NCL at $p' = 1$ kPa, $\lambda = 0.177$ is the gradient of normal compression line. The compression curve of the disaggregated sandstone specimen does not seem to converge on the NCL of the cemented one, but rather located on the right of this line, which is similar to the case of weak cement bonds as described by Cuccovilo and Coop.[9]

When comparing the compression curves of cemented and disaggregated samples of similar initial specific volumes, the disaggregated material does not yield until higher stress levels as it will be shown later that particle breakage does not happen in this stress range and the bonds are already broken from the beginning of the test. The remaining mechanisms for volume compression of the disaggregated material are particle rearrangement and deformation of weak cement particles, which are less significant as compared to breakage of cement bonds of the cemented sandstone. The yield stress of the cemented sandstone is due to bond breakage or bond yield and it is in lower stress range as the silica

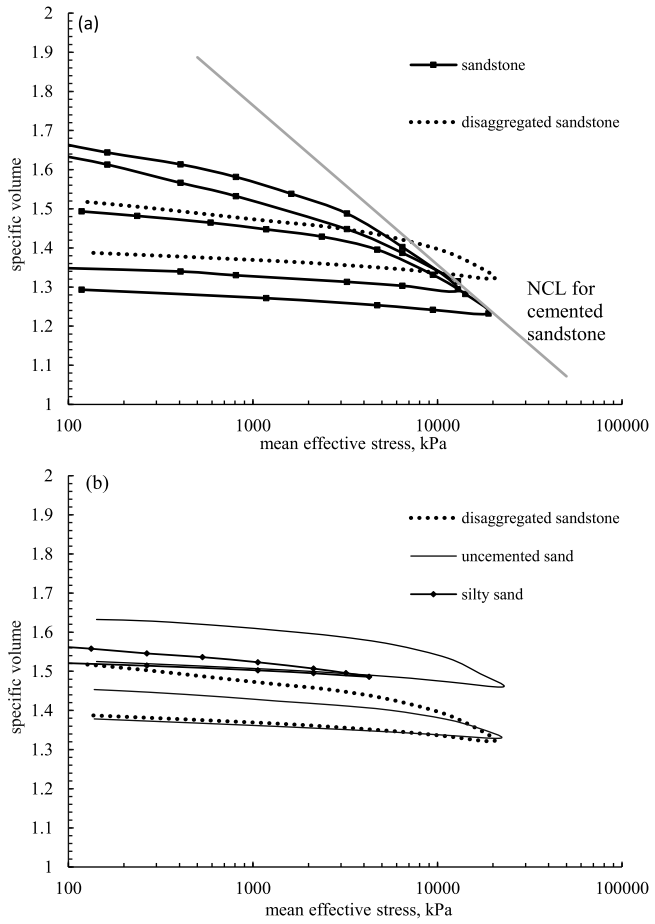

Fig. 4. One-dimensional compression of: (a) cemented sandstone and (b) uncemented sand.

cement bonds are weak as shown in Fig. 2b. The unloading paths for the cemented and the disaggregated materials are parallel indicating similar behavior and conclusion that the majority of the cement bonds in the cemented sandstone samples have been broken after the yield points.

Fig. 4b shows the compression curves of uncemented materials including sand, disaggregated sandstone and silty-sand samples. The silty sand material was prepared to have the same mixing proportion of sand particles and of fine particles that are of the same sizes as the cement particles and hence it has similar particle size distribution to the disaggregated sandstone but of different mineralogy for the fine particles. None of the compression curves of the uncemented materials converge on a unique NCL in the tested stress range in Fig. 4b, the dense and loose sand samples form parallel curves to each other. The sand samples were checked by the Qicpic equipment before and after the oedometer test. The results of the particle aspect ratio and size distribution in Fig. 5 indicate no significant change in the particle shape and size and hence particle breakage is negligible. The non-convergence of the compression curves in Fig. 4b could be due to the lack of particle breakage for the uncemented materials tested within the limited stress ranges of our equipment in the laboratory.

Volume compression of granular materials is usually related to particle breakage and the threshold stress level that initiates the acceleration of grain fracture is considered as the yield stress.[27,32,37] If the grains are strong and difficult to deform, the applied energy is mostly directed to the friction loss and to the work on bonding breakage.[8] As the bonds break and the grains start to slide and roll, the cemented structure starts to degrade and the cemented material is transformed from a structured material to a frictional material.[3] Our analysis of the grains after the compression tests revealed that the sand grains remained intact with no significant breakage. This implied that the apparent yield stress in Fig. 4a is mostly associated with the bond breakage. At the yield stress, the "bridge" shaped cement bonds in Fig. 2b could break and fall into intergranular voids as silicate cement is highly deformable. Bond breakage will cause significant grains rearrangement leading to the convergence of the NCL as shown in Fig. 4a for the cemented sandstone.

4. Shearing

4.1. Pre-failure behavior

Stiffness is an important parameter employed in the explicit analysis of the recoverable reserves of the reservoir prior to the start of hydrocarbon production.[38] Confining pressure may affect the stiffness of the material and the tangential shear modulus during shearing of cemented samples was calculated from the ratio of the deviatoric stress increment over the corresponding strain increment for small strain intervals.[39] The results for samples of different confining pressures are plotted against the deviatoric stress in Fig. 6.

Fig. 6 shows that the initial tangential modulus is constant and does not depend on the confining pressure until a threshold deviatoric stress level when it starts to degrade. This stress level depends on the confining pressure. The initial modulus of about 1300 MPa is slightly less than the value of the weak sandstone discussed in the work of Altuhafi and Coop[3] which is composed of strong silica grains that are weakly bonded by iron oxide cement. As shearing progresses, the cemented structure degrades and the material is gradually transformed from a structured material to a frictional material. The stress level where the modulus decreases is considered as the yield stress when the bond breakage occurs. The sandstone in the study of Altuhafi and Coop[3] is classified as weak sandstone but is stronger than our material in terms of both the higher yield stress and the higher initial modulus value. As the initial modulus of the materials is fairly constant, the cemented structure has a dominant role in this stress range before the bond breaks. The value of the initial modulus should be governed by the deformability of the intact bonds and with the smaller initial modulus value, the silica cement bonds in our materials could be more deformable than the iron oxide cement in the study by Cuccovillo and Coop.[3]

The bond breakage behavior before the peak strength is further investigated on a cemented sample (B850) which was tested under a constant mean stress and several unloading–reloading stress probes were conducted at small strain levels. The results in Fig. 7 show that the unloading–reloading curves are linear at strain levels less than 0.5% but at larger axial strain around 1%, the unloading–loading behavior becomes non-linear which indicates plastic behavior due to bond breakage and/or particle rearrangement. Bond breakage hence starts much earlier than the peak strength, which was usually measured at around 2% of axial strain.

4.2. Failure behavior

The stress–strain curves of the cemented sandstone samples sheared at low to medium confining pressures p_c from 200 kPa to 400 kPa are shown in Fig. 8. The results are compared to two other artificial materials, one of the same sand particle mineralogy but with a stronger cement[40] and another material of

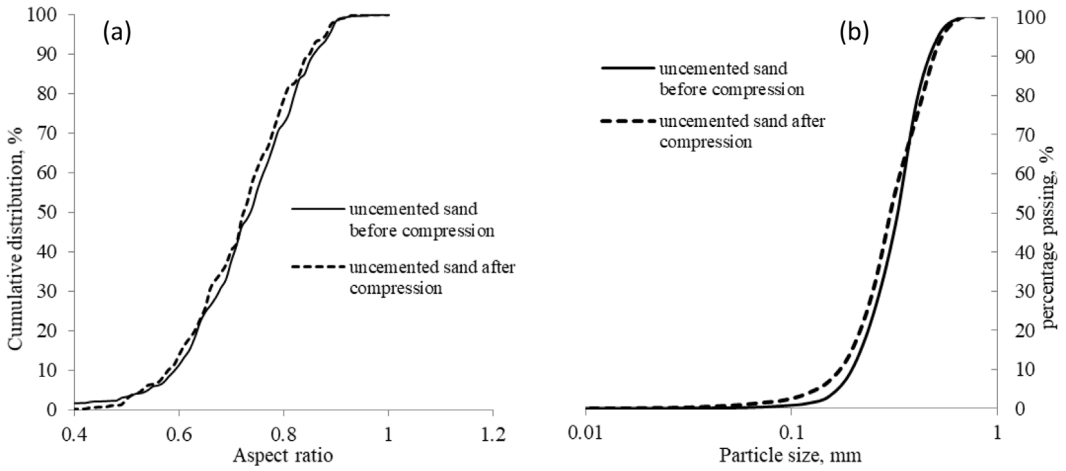

Fig. 5. (a) Particle aspect ratio, (b) Particle size distribution of sand samples before and after compression tests.

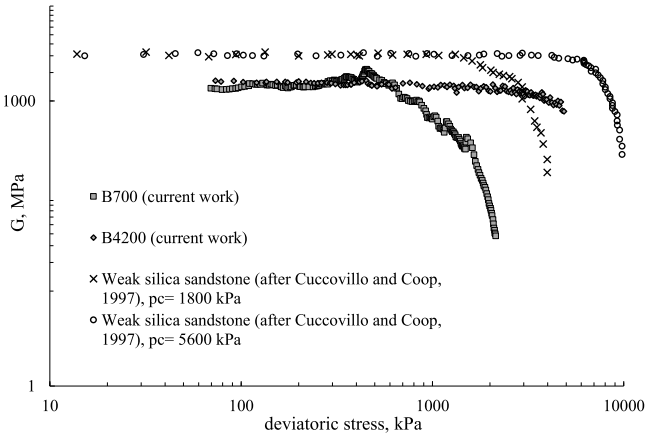

Fig. 6. Shear modulus of artificial cemented sandstone.

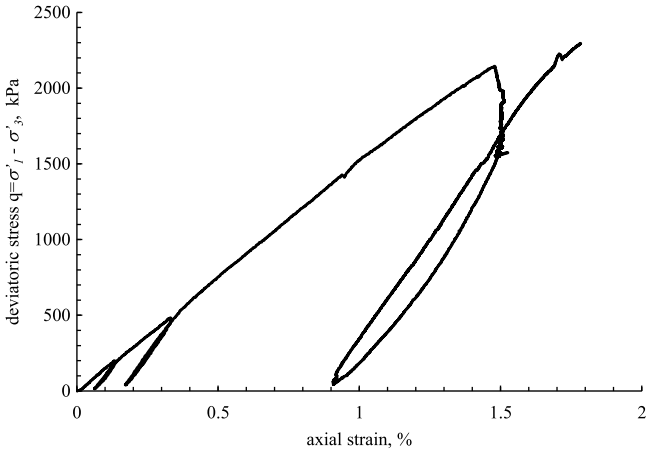

Fig. 7. Small-strain shear probes on the pre-peak behavior of sample B850.

the same cement type but with weaker sand particles.[41] Further information on the sand particles and the type of cement bonds of three materials are given in Table 2. While the Quartz sand and Portland cement are considered as strong particles and strong cement, the Feldspar sand and sodium gel are considered as weak particles and weak cement leading to three different classifications of particle–cement systems of strong–strong (particle–cement), weak–weak and strong–weak as shown in Table 2.

For comparison with current work, only selected samples of similar confining pressure and cement content from Refs. 40, 41 are shown in Fig. 8. With a strong cement, the Quartz sand particles form a stronger sandstone material in Ref. 40 that have the maximum deviatoric strength of about 1.2 to 1.5 times higher than the deviatoric strength of the artificial sandstone in the current study. The critical state strength however is similar to the critical strength of our material and the effects of the cement bonds diminish at large deformation as the materials become mainly frictional. The higher stiffness of the strong–strong material in Fig. 8 is due to the stronger cemented structure, which has a dominant role in the pre-peak stress range. The weak–weak sandstone in the study by Porcino and Marciano[41] has a significantly lower peak strength, which is also less pronounced, and a lower stiffness, which could be due to bond breakage occurring earlier and more gradually in the shearing process. The critical state strength of weak–weak sandstone is lower, which indicates a different frictional resistance for the Feldspar

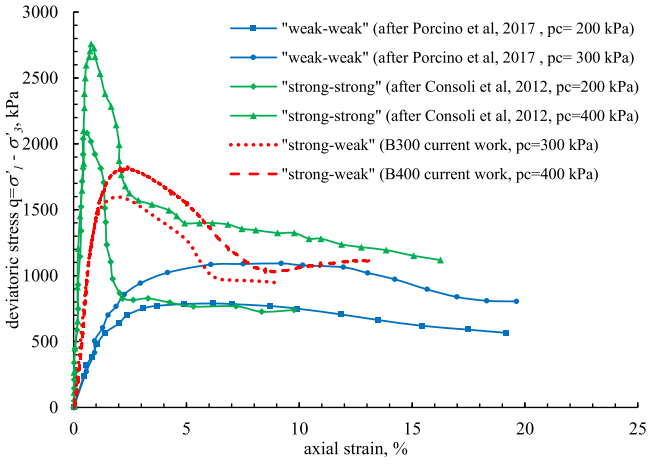

Fig. 8. Stress–strain behavior of artificial sandstones.

sand particles and it could also be attributable to a change in the particle size distribution during shearing for this material. The sand particles and the cement both affect the strength and deformational characteristics of the sandstones, the behaviors of which are shown to be significantly stronger and more brittle when the materials are constituted by the stronger particles and cement types.

Table 2
Particle mineralogy and cement types of different artificial sandstone materials.

Particle–cement classification	Strong–strong	Weak–weak	Strong–weak
Reference	Consoliet al.[40]	Porcino & Marcianò,[41]	Current work
Sand material	Osario fine sand (Brazil)	Ticino silica sand (Italy)	Open quarry sand (Kazakhstan)
Particle mineralogy	Predominantly quartz	Quartz - 30%; feldspar - 65% ; mica - 5%	Predominantly quartz
Cement material	Portland cement	Sodium gel	Sodium silicate solution (sodium gel)

Fig. 9 shows the stress ratio and volumetric strain results of the uncemented and cemented materials in this study. At the critical state of around 10% axial strain, the curves of both cemented and uncemented specimens converge to a same stress ratio value, indicating the effects of cementation were eradicated and all samples behave as a frictional material. The frictional resistance of which can be quantified by a critical state parameter value of $M = 1.47$ as shown in Fig. 9a. The shearing of sample B4200 was stopped short of the critical state as of other samples and this is due to the apparatus limitation in this test but extrapolation of the stress ratio curve tends to go to the same stress ratio. The peak stress ratios of cemented samples are higher than of uncemented sample and this is the effect of the cement bonds. Sample B300 has the highest peak stress ratio value although this sample dilates less than sample B400 in Fig. 9b. A higher dilation of sample B400 despite having a higher confining pressure could be due to the lower initial void ratio of this sample as shown in Table 1. An uncemented sample of higher dilatancy would achieve higher peak stress ratio as the peak strength is associated with the sample's dilatancy but this is not true for the cemented samples B300 and B400 as the higher peak strength is attributable to the bonded structure. Sample B4200 does not exhibit a peak strength and this is the behavior of a loose sample combined with the effect of a high confining pressure. Sample B4200 was trimmed to a smaller size for the high pressure test and the measured initial void is significantly higher than the other samples indicating that volume expansion and possible bond breakage would occur for this sample before the shear stage. Furthermore, shearing behavior of cemented materials at high confining pressures can be dominated by frictional resistance as it has been observed by Consoli et al.[40] Fig. 9b shows that the samples usually contracted to about 1% of volumetric strain before exhibiting a dilative behavior. The dilatancy happens simultaneously with bond breakage and the cemented samples tend to dilate more than the uncemented sample in Fig. 9b, which agrees with the observation by Cuccovillo and Coop.[3,9]

Fig. 10 shows the shear strength envelopes for the cemented and uncemented samples. The peak strengths of the cemented samples fall onto a unique peak strength envelope, while the critical strengths of all samples fall on another critical state strength envelope, which corresponds to the critical parameter $M = 1.47$. The peak strength of the uncemented sample also falls on the critical state line, which is the result of loose sand. The peak strength envelope crosses the vertical axis at a cohesion value, which reflects the effect of cementation for this material. As the critical state line is the same for both cemented and uncemented samples, the effect of cementation ceases and major bond breakage should have already happened before the critical state.

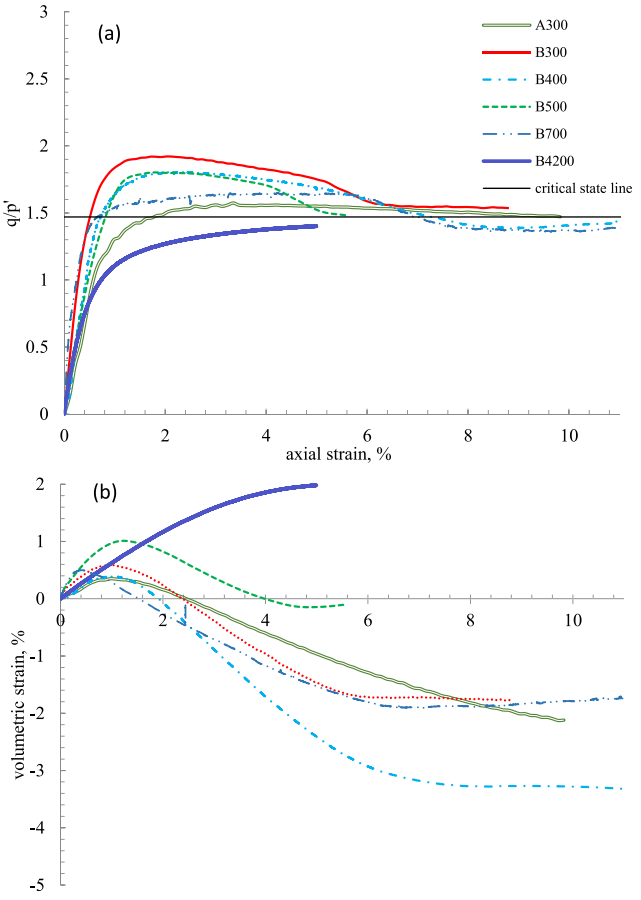

Fig. 9. (a) Stress ratio (b) Volumetric strain behavior of uncemented and cemented materials in this study.

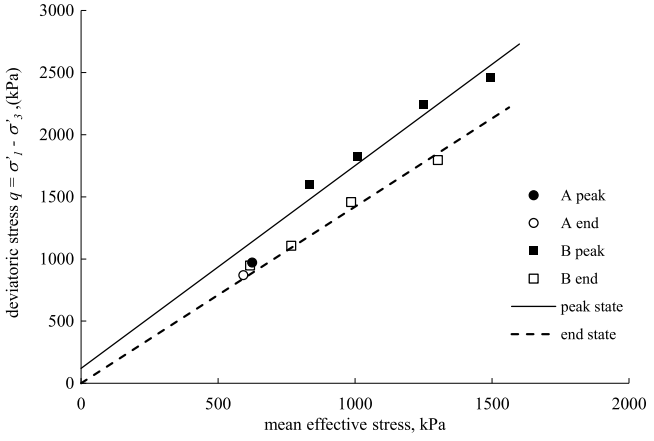

Fig. 10. Peak strength and critical state strength envelopes of the artificial sandstone.

5. Discrete element method simulation of weak sandstone behavior

Discrete element method (DEM) simulation was conducted to simulate the behavior of the artificial sandstone in this study due to the difficulties associated with quantitative examination of the bond breakage behavior in the experiments. Sandstone is simulated as an assembly of spherical particles that are

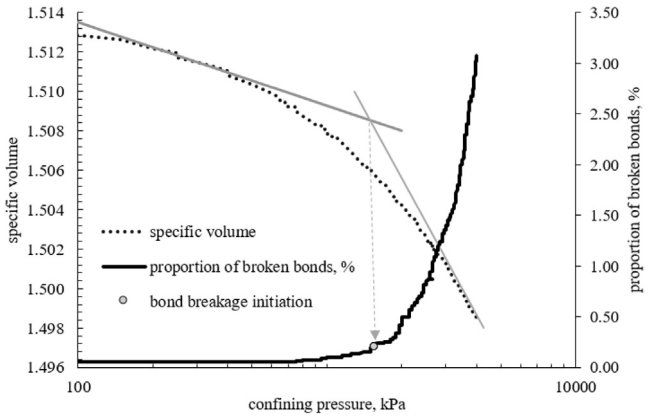

Fig. 11. Bond breakage during isotropic compression in the numerical simulation.

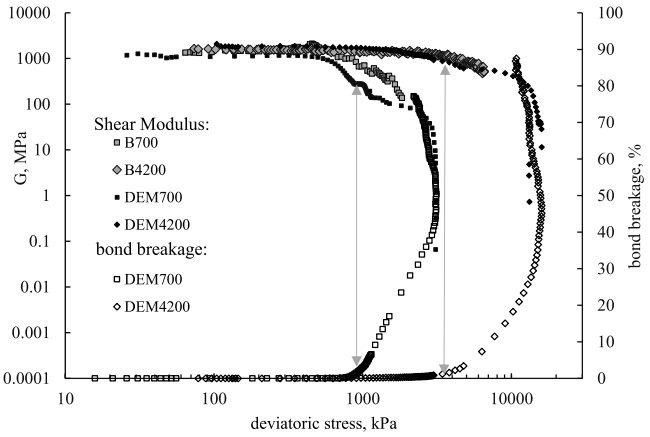

Fig. 12. Bond breakage during shearing of numerical samples.

bonded together by a contact bond model that was developed by Rakhimzhanova et al.[16,17] The contact bond model was an adaptation of the Johnson–Kendal–Roberts (JKR)[15] theory for auto-adhesive particles such that cement bonds were only formed once at the beginning of the consolidation process and they can be broken and will not bond again during the subsequent stages of consolidation and shear.

The numerical particles are generated in the simulation following the same size distribution of the real material in the laboratory experiments. A total number of 5942 spherical particles were randomly generated inside a 4.9 mm × 4.9 mm × 4.9 mm cubic cell bounded by periodic boundaries to form a gas-like initial state. The particles were brought into contact by shrinking the cell until an initial isotropic stress state was developed and the contact bonds were then activated at the already-formed interparticle contacts. The numerical samples are considered in the intact state in this condition when they are subjected to further consolidation and shear loading stages as similar to the experimental conditions. The bonds were formed only once during isotropic compression and could break when the contact force conditions satisfy the bond breakage criterion. Once the bonds break, new contacts can be formed; the behavior at which is no longer affected by the bonds, and hence is governed by the Hertz–Mindlin contact model. Further details on the contact model and the simulation procedure can be found in Rakhimzhanova et al.[16,17] The input parameters were calibrated for the weak sandstone by varying the value of the interparticle cohesion Γ. A good agreement with the experimental results is achieved with the following main input parameters: Young's modulus E = 70 GPa, Poisson's ratio $\nu = 0.3$, interparticle cohesion $\Gamma = 20$.

Fig. 11 shows the compression curve and bond breakage behavior during the initial isotropic compression (consolidation) in the numerical simulation. Volume contraction of the numerical sample happens more gradually and no distinct yield stress can be identified from the curve where it is estimated at the intersection of the two tangential lines drawn to the beginning and the end of the compression curve. The bond breakage behavior is also overlaid on the same figure, showing that bond breakage starts accelerating beyond the yield stress and hence it is evidenced from the DEM simulation that yield stress during compression of cemented sandstone is related to the bond breakage initiation and this supports the experimental results in Fig. 4. In general, bond breakage during isotropic compression is not significant as only 3% of bonds are broken at 4000 kPa. The majority of bond breakage will occur during shearing as it will be shown later.

The tangential shear modulus of numerical samples is plotted in Fig. 12 and similar to Fig. 11, the percentages of the broken bonds are superimposed on the same figure. The initial tangential shear modulus of the numerical samples agrees well with the experimental results and it is now clear from the simulation results that the decrease of the initial modulus is associated with the initiation of bond breakage. Bond breakage is much more significant during shearing as compared to the compression stage, 80% to 90% of the bonds inside the numerical samples are broken at the end of the shear test. In the lack of particle breakage, the pre-failure behavior of cemented sandstone is controlled by the cement bonds and the breakage of the cement bonds mark a transition in the material behavior from a structure-dominant state to a frictional dominant state as it has been discussed in previous study and is explicitly observed in our numerical simulation results.

5.1. Failure behavior

The stress–strain behaviors of the numerical samples during shearing are compared to the experimental results in Fig. 13 for different confining pressures. The numerical stress ratio curves attain a peak value at around 4%∼5% of axial strain which is followed by a softening behavior to a residual stress ratio A horizontal plateau at large strain levels as in Figs. 8 and 9 for real materials are not observed in the numerical simulation. Fig. 13b shows that the numerical samples expand their volumes much higher than the experimental results; note that volume contraction is positive following the usual soil mechanics convention. This could be due to plastic deformation of the cement material and sand particles, which is not considered in the simulation. The numerical samples continue expanding its volume at the end of the shearing process and the critical state as defined by a constant volume and stress ratio is not strictly achieved in this case. The peak strength envelopes of both numerical and experimental samples are plotted in Fig. 14 showing an excellent agreement between the two results within the range of the confining pressures in the study.

The effect of confining pressure on bond breakage behavior is shown in Fig. 15. For samples of lower confining pressures, initial bond breakage happens quickly within the range below 4% of the axial strain and before the peak strength (i.e., DEM300) and then wanes with decreasing bond breaking rates. Bond breakage at higher confining pressures (i.e. DEM4200) on the other hand occurs more gradually before the peak strength but keeps increasing at the same rate after the peak strength. As bond breakage occurs more gradually for higher confining pressures, it would be less distinct for the transition from a structure dominant behavior to

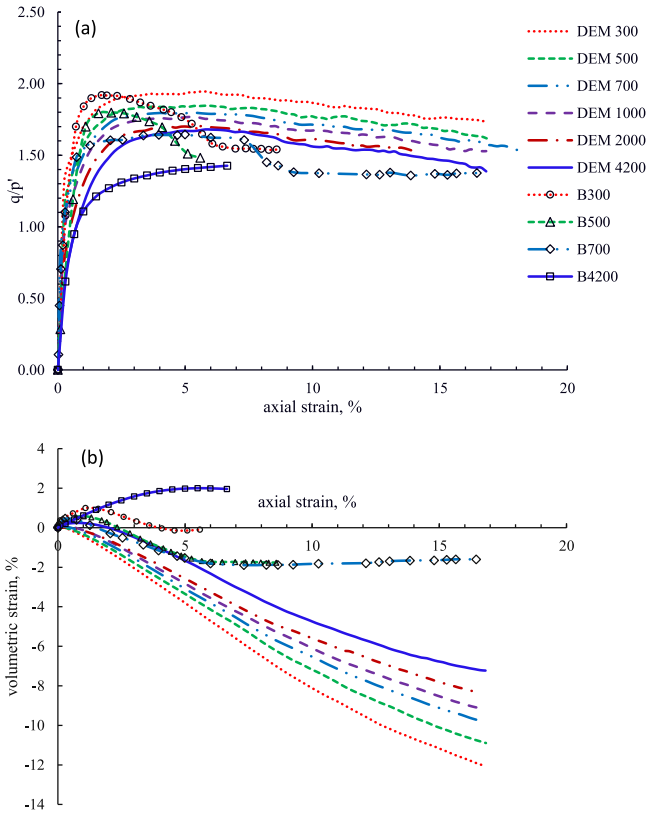

Fig. 13. (a) Stress ratio (b) Volumetric strain behavior of the numerical and experimental samples.

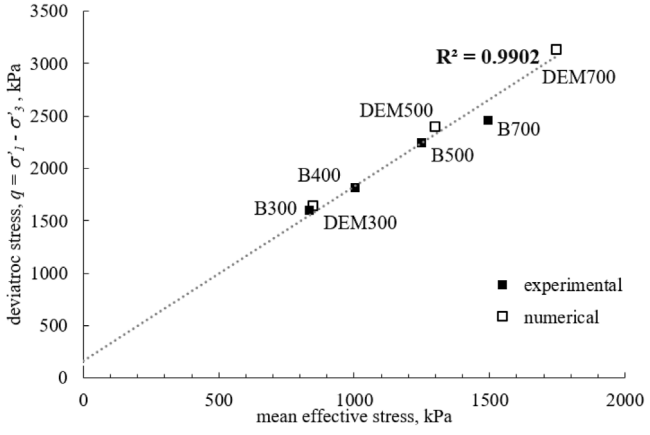

Fig. 14. Peak strength envelope of experimental and numerical samples.

a frictional dominant behavior and we may expect a less distinct peak stress ratio for these samples.

Fig. 16 shows the results of bond breakage percentage against the stress ratio value during shearing. Sample DEM4200 attains a lower maximum stress ratio of 1.7 at a lower percentage of bond breakage of 45% as compared to a maximum stress ratio of 2.0 and a bond breakage of 55% for DEM300. These results support the previous conclusion that higher confining pressure would decrease the effect of cement bonds and of the material's structure and promote the effect of the frictional resistance at the contacts between particles. It is also noted that DEM4200 attains a higher final bond breakage percentage than DEM300 at the end of the test and the numerical samples do not attain the same critical stress ratio. A unique critical state is hence not achieved for the

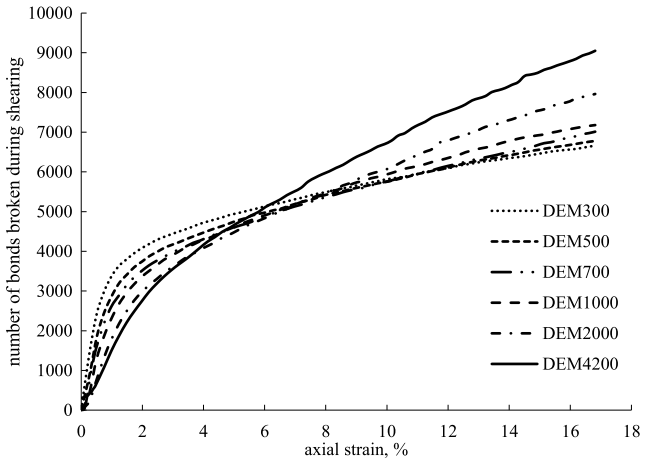

Fig. 15. Bond breakage behavior at different confining pressures.

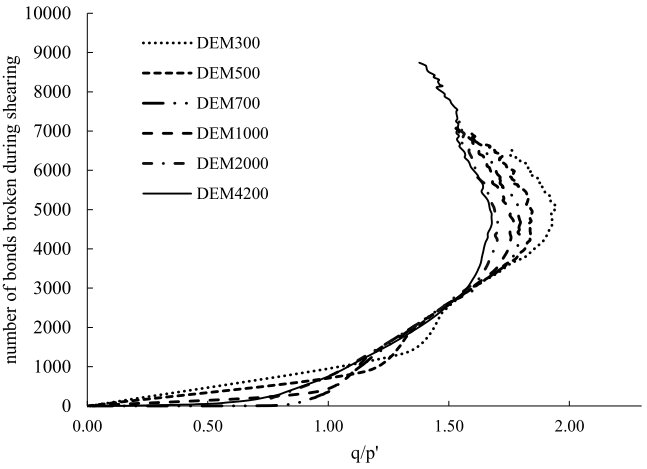

Fig. 16. Bond breakage against stress ratio of numerical samples.

numerical samples as in the experimental results and this could be a limitation of the simulation method and the contact bond model when it does not take into account the plastic deformation of contact bonds and the full microscopic properties of the sand particles and cement material. The behavior of bond breakage is important for the prediction of wellbore instability and analysis, especially for the wells within similar strata but with different depths. The lower confining pressures at shallower depths would imply a more sudden strength loss at small strains leading to shorter time window for response and/or more restriction to the control of reservoir deformation to guarantee wellbore stability.

6. Conclusion

The behavior of weak sandstone reservoir materials in Kazakhstan was investigated using experimental and numerical methodologies. Artificial sandstone replicating the real reservoir materials was created in the laboratory by mixing sand of a similar mineralogy and particle size distribution with a silica sodium cementing agent. The materials were hardened when the cement material reacted chemically with the carbon dioxide gas injected into the specimen's chamber under controlled condition. Compression test and shear test were conducted on the artificial sandstone specimens and the results were compared to the DEM simulation results of similar testing conditions. It was found that weak porous sandstone compressibility, which plays a significant

role in oil production estimation, majorly depends on the bonding stiffness and is constant until a threshold deviatoric stress level. The plastic yielding condition of the weak sandstone was also found to be closely related to the bond breakage behavior. Due to the strong quartz sand particles and the weak silica cement, particle breakage did not happen during the test and this is confirmed by comparing the particle size distribution and particle aspect ratio statistics before and after the test where no significant change was observed. Cement bonds however break and constitute the mechanism for volume compression of the cemented material. A unique Normal Compression Line was observed for the cemented sandstone but not for the uncemented sand within the applied stress ranges of our equipment. In shear tests, the specimen stiffness degrades as soon as the cement bonds break and the material behavior is transformed from a structure-dominant state to a friction-dominant state as it approaches the failure conditions. Cemented samples can attain different peak strengths with different cemented structures. However, the cemented samples have the same critical state strength of the uncemented sands when the bonds were broken and the resistance is solely attributable to the frictional resistance between sand particles. The soft broken cement materials filling in the voids do not affect the critical state of the otherwise uncemented sand at large deformation. The simulation results support the experimental observations by relating the plastic yielding behavior directly to the initiation condition of bond breakage. Higher confining pressures lead to smaller bond breakage percentage at the peak stress ratio and less rapid change in the bond breakage rate at the start of the shearing process. These affected the failure behavior of the cemented material.

The consistency between the experimental and numerical results confirm that the majority of bond breakage occurs before and around the peak strength for samples at lower confining pressures. The material behavior has a significant implication for the prediction of wellbore instability and sand production behavior for the shallow formations in Kazakhstan. A series of sand production experiment on the same synthetic material is being carried out to investigate the effect of the strength and deformational characteristics of the material on the volume of produced sand and sanding rate under realistic stress and flow conditions.

Acknowledgments

The authors acknowledge the financial support from Nazarbayev University (research grant SOE2015004) and the generous support we received from overseas collaborating laboratories during the research. The authors are also grateful to Ms. Aigerim Rakhimzhanova for the training for the DEM simulation in this work.

References

1. Airey DW. Triaxial testing of naturally cemented carbonate soil. *J Geotech Eng*. 1993;119(9):1379–1398.
2. Coop MR, Atkinson JH. The mechanics of cemented carbonate sands. *Géotechnique*. 1993;43(1):53–67. http://dx.doi.org/10.1680/geot.1993.43.1.533.
3. Cuccovillo T, Coop MR. Yielding and pre-failure deformation of structured sands. *Géotechnique*. 1997;47(3):491–508. http://dx.doi.org/10.1680/geot.1997.47.3.491.
4. Dobereiner L, Freitas MH. Geotechnical properties of weak sandstones. *Géotechnique*. 1986;36(1):79–94. http://dx.doi.org/10.1680/geot.1986.36.1.79.
5. Atapour H, Mortazavi A. The effect of grain size and cement content on index properties of weakly solidified artificial sandstones. *J J Geophys Eng Geophys Eng*. 2017. http://www.ncbi.nlm.nih.gov/pubmed/21410437.
6. Atapour H, Mortazavi A. The influence of mean grain size on unconfined compressive strength of weakly consolidated reservoir sandstones. *J Pet Sci Eng*. 2018;171(June):63–70. http://dx.doi.org/10.1016/j.petrol.2018.07.029.
7. Burland JB. On the compressibility and shear strength of natural clays. *Géotechnique*. 1990;40(3):329–378. http://dx.doi.org/10.1680/geot.1990.40.3.329.
8. Wang YH, Leung SC. Characterization of cemented sand by experimental and numerical investigations. *J Geotech Geoenviron Eng*. 2008;134(July 2008):992–1004. http://dx.doi.org/10.1061/(ASCE)1090-0241(2008)134:7(992).
9. Cuccovillo T, Coop MR. On the mechanics of structured sands. *Géotechnique*. 1999;49(6):741–760. http://dx.doi.org/10.1680/geot.1999.49.6.741.
10. Alvarado G, Coop MR, Willson S. On the role of bond breakage due to unloading in the behaviour of weak sandstones. *Géotechnique*. 2012;62(4):303–316. http://dx.doi.org/10.1680/geot.8.P.017.
11. Cundall PA, Strack ODL. Discussion: A discrete numerical model for granular assemblies. *Géotechnique*. 1979;29:47–65. http://dx.doi.org/10.1680/geot.1980.30.3.331.
12. Nova R, Castellanza R, Tamagnini C. A constitutive model for bonded geomaterials subject to mechanical and/or chemical degradation. *Int J Numer Anal Methods Geomech*. 2003;27(9):705–732. http://dx.doi.org/10.1002/nag.294.
13. Utili S, Nova R. DEM Analysis of bonded granular geomaterials. *Int J Numer Anal Methods Geomech*. 2008;32:1997–2031. http://dx.doi.org/10.1002/nag.72814.
14. Shen Z, Jiang M, Thornton C. DEM Simulation of bonded granular material. Part I: Contact model and application to cemented sand. *Comput Geotech*. 2016;75:192–209. http://dx.doi.org/10.1016/j.compgeo.2016.02.007.
15. Johnson KL, Kendall K, Roberts AD. Surface energy and the contact of elastic solids. *Proc R Soc A Math Phys Eng Sci*. 1971;324(1558):301–313. http://dx.doi.org/10.1098/rspa.1971.0141.
16. Rakhimzhanova AK, Khamitov FA, Minh NH, Thornton C. 3D DEM simulations of triaxial compression tests of cemented sandstone. In: *Proceedings of IS Atlanta 2018 Symposium on Geomechanics from Micro to Macro in Research and Practice*, Atlanta, USA; 2018.
17. Rakhimzhanova AK, Thornton C, Minh NH, Fok SC, Zhao Y. Numerical simulations of triaxial compression tests of cemented sandstone. *Comput Geotech*. 2019;113(January). 103068. http://dx.doi.org/10.1016/j.compgeo.2019.04.013.
18. Brok S, den David C, Bernabé Y. Preparation of synthetic sandstones with variable cementation for studying the physical properties of granular rocks. *C R Acad Sci IIA*. 1997;325(7):487–492. http://dx.doi.org/10.1016/S1251-8050(97)89866-7.
19. David C, Menéndez B, Bernabé Y. The mechanical behaviour of synthetic sandstone with varying brittle cement content. *Int J Rock Mech Min Sci*. 1998;35(6):759–770. http://dx.doi.org/10.1016/S0148-9062(98)00003-5.
20. Holt RM, Kenter C. Simulation of core damage induced by stress release. 1992, p. 959–968.
21. Holt RM, Unander TE, Kenter CJ. Constitutive mechanical behaviour of synthetic sandstone formed under stress. *Int J Rock Mech Min Sci*. 1993;30(7):719–722. http://dx.doi.org/10.1016/0148-9062(93)90013-4.
22. D 2487-98 ASTM. ASTM. Standard practice for classification of soils for engineering purposes (unified soil classification system) D 2487-98, ASTM. *ASTM Stand Pract Classif Soils Eng Purp (Unified Soil Classif Syst D)*. 1998;2487–2498, ASTM.:2487.
23. Altuhafi F, Baudet BA, Sammonds P. The mechanics of subglacial sediment: an example of new transitional behaviour. *Can Geotech J*. 2010;47(7):775–790. http://dx.doi.org/10.1139/T09-136.
24. Consoli NC, Winter D, Rilho AS, Festugato L, Teixeira B, dos S. A testing procedure for predicting strength in artificially cemented soft soils. *Eng Geol*. 2015;195:327–334. http://dx.doi.org/10.1016/j.enggeo.2015.06.005.
25. Rios S, Viana da Fonseca A, Baudet BA. On the shearing behaviour of an artificially cemented soil. *Acta Geotech*. 2014;9(2):215–226. http://dx.doi.org/10.1007/s11440-013-0242-7.
26. Kozhagulova AA, Shabdirova AD, Minh GT, Bond NH. Characteristics of artificial sandstones with sodium silicate cement. In: *52nd US Rock Mechanics/Geomechanics Symposium*, Seattle, Washington 2018.
27. Altuhafi F, Coop MR. Changes to particle characteristics associated with the compression of sands. *Géotechnique*. 2011;61(6):459–471. http://dx.doi.org/10.1680/geot.9.P.114.
28. BS 1377. British Standard Institution. Methods of Test for Soil for Civil Engineering Purposes, BS 1377, 1990.
29. Skempton aW. The pore-pressure coefficients A and B. *Géotechnique*. 1954;4(4):143–147. http://dx.doi.org/10.1680/geot.1954.4.4.143.
30. Rocchi I, Coop MR. Experimental accuracy of the initial specific volume. *Geotech Test J*. 2014;37(1). http://dx.doi.org/10.1520/GTJ20130047.
31. La-Rochelle P, Leroueil S, Trak B, Blais-Leroux L, Tavenas FA. Observational approach to membrane and area corrections in triaxial tests. *Adv Triaxial Test Soil Rock*. 1988;715–731. http://dx.doi.org/10.1016/0148-9062(91)92767-S.
32. Coop MR, Lee IK. The behaviour of granular soils at elevated stresses. *Predict Soil Mech*. 1993;(1990):186–198.
33. Ghafghazi M, Shuttle DA, DeJong JT. Particle breakage and the critical state of sand. *Soils Found*. 2014;54(3):451–461. http://dx.doi.org/10.1016/j.s{and}f.2014.04.016.

34. Mesri G, Vardhanabhuti B. Compression of granular materials. *Can Geotech J.* 2009;46(4):369–392. http://dx.doi.org/10.1139/T08-123.
35. Jaky J. The coefficient of earth pressure at rest. *Sot Hung Arch Eng.* 1944;22:355–358.
36. Yamamuro JA, Bopp PA, Lade PV. One-dimensional compression of sands at high pressures. *J Geotech Eng.* 1996;122(2):147–154.
37. McDowell GR, Bolton MD. Discussion: On the micromechanics of crushable aggregates. *Géotechnique.* 1998;48(5):667–679. http://dx.doi.org/10.1680/geot.2000.50.3.315.
38. Dake LP. *The Practice of Reservoir Engineering.* revised ed., Elsevier; 2004, http://dx.doi.org/10.1016/0920-41050(95)00060-7.
39. Atkinson JH, Richardson D, Woods RI. Note on the determination of tangent stiffness parameters from soil test data. *Comput Geotech.* 1986;2:131–140.
40. Consoli NC, Cruz RC, Fonseca AV, Coop MR. Influence of cement-voids ratio on stress-dilatancy behavior of artificially cemented sand. *J Geotech Geoenviron Eng.* 2012;138(1):100–109. http://dx.doi.org/10.1061/(ASCE)GT.1943-5606.0000565.
41. Porcino DD, Marcianò V. Bonding degradation and stress–dilatancy response of weakly cemented sands. *Geomech Geoengin.* 2017;12(4):221–233. http://dx.doi.org/10.1080/17486025.2017.1347287.